ISBN: 978-3-95450-236-3 ISSN: 2673-5350 doi:10.18429/JACoW-IBIC2023-WE3I01

GAS JET BASED FLUORESCENCE PROFILE MONITOR FOR LOW ENERGY ELECTRONS AND HIGH ENERGY PROTONS AT LHC

O. Sedlacek*[1], O. Stringer, C. Welsch, A. Webber-Date, H. Zhang
University of Liverpool and Cockcroft Institute, Daresbury, Warrington, UK
M. Ady, A. R. Churchman, S. Mazzoni, A. Rossi, M. Sameed, G. Schneider,
C. C. Sequeiro, K. Sidorowski, R. Veness, CERN, Geneva, Switzerland
P. Forck, S. Udrea, GSI, Darmstadt, Germany
[1] also at CERN, Geneva, Switzerland

Abstract

The ever-developing accelerator capabilities of increasing beam intensity, e.g. for High Luminosity LHC (HL-LHC), demand novel non-invasive beam diagnostics. As a part of the HL-LHC project a Beam Gas Curtain monitor (BGC), a gas jet-based fluorescence transverse profile monitor, is being developed. The BGC uses a supersonic gas jet sheet that traverses the beam at 45° and visualizes a two-dimensional beam-induced fluorescent image. The principle of observing photons created by fluorescence makes the monitor insensitive to present electric or magnetic fields. Therefore, the monitor is well suited for high-intensity beams such as low-energy electron beam of Hollow Electron Lens (HEL), and HL-LHC proton beam, either as a profile or an overlap monitor. This talk will focus on the first gas jet measured transverse profile of the 7 keV hollow electron beam. The measurements were carried out at the Electron Beam Test Stand at CERN testing up to 5 A beam for HEL. A comparison with Optical Transition Radiation measurements shows consistency with the BGC results. The BGC installation of January 2023 at LHC is shown, including past results from distributed gas fluorescence tests.

INTRODUCTION

The High Luminosity upgrade of the LHC (HL-LHC) aims at extending its operability by a decade by increasing its instantaneous luminosity by a factor of five beyond its present design value [1]. The main feature of HL-LHC is the upgrade of the focusing triplets to allow for a smaller β^* in the interaction region, combined with compact superconducting radio frequency crab cavities for bunch rotation. For these systems to operate safely, a Hollow Electron Lens (HEL) is being studied to improve the cleaning performance of the collimation system. Optimal performance of the HEL requires a means to measure the relative position of the hollow, low-energy electron beam with respect to the LHC proton beam in a non-invasive way. It is in this context, a collaboration between CERN, University of Liverpool and GSI was established to design and produce a Beam Gas Curtain (BGC) as an overlap monitor for the HEL [2–7]. The strategy for commissioning the BGC consists of a parallel validation of its performance in both the Electron Beam Test Stand (EBTS) [8] and the LHC during the present run 3. In this contribution, we report on the recent progress of the BGC at the EBTS and present the configuration of the ongoing LHC installation.

* Ondrej.Sedlacek@cern.ch

BGC INSTRUMENT

Principle of Detection

The BGC working principle is outlined in Fig. 1. The monitor is based on a flat, supersonic gas jet referred to as a "curtain", which perpendicularly crosses the beams' path with the flat edge at 45° with respect to the horizontal plane (see Fig. 1). The beams excite the gas atoms or molecule through collisions. Subsequent radiative deexcitation leads to photon emission (fluorescence). The fluorescence footprint on the gas curtain thus directly relates to the particle beams' 2D transverse particle distributions, allowing for the observation of the beams' 2D transverse profiles in a non-invasive way.

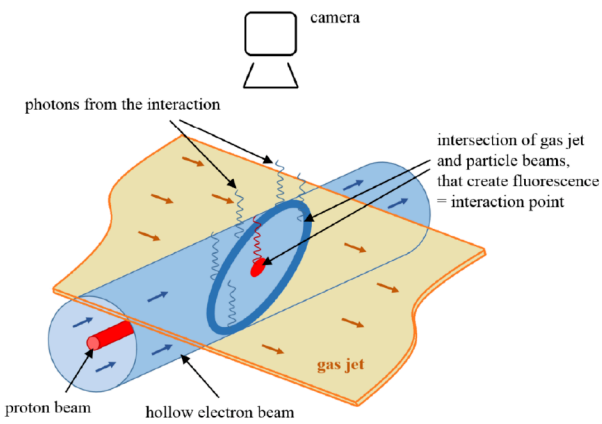

Figure 1: Working principle of the BGC.

Working Gas

Neon, nitrogen, and argon have been selected as working gases for the BGC, each presenting advantages and disadvantages that affect the monitor's performance. Their fluorescence processes are described in Eqs. (1)–(3):

$$Ne + p/e^- \rightarrow (Ne)^* + p/e^- \rightarrow Ne + \gamma + p/e^- \quad (1)$$

$$N_2 + p/e^- \rightarrow (N_2^+)^* + e^- + p/e^- \rightarrow N_2^+ + \gamma + e^- + p/e^- \quad (2)$$

$$Ar + p/e^- \rightarrow (Ar^+)^* + e^- + p/e^- \rightarrow Ar^+ + \gamma + e^- + p/e^- \quad (3)$$

ISBN: 978-3-95450-236-3 ISSN: 2673-5350 doi:10.18429/JACoW-IBIC2023-WE3I01

Neon gas curtains have the highest density. However, neon has the lowest (expected) cross-sections and light yields. At the same time, the relevant transition takes place within the neutral atom, see Eq. (1) at 585.4 nm [9, 10]. Therefore, it is not affected by the beam's space charge during the atom's fluorescence lifetime[1] of 16 ns. Additionally, neon and argon are a noble gases and, as such, they don't saturate the Non-Evaporable Getter (NEG) coating often present at LHC [10].

Nitrogen gas jets have the highest light yields. Its strongest fluorescence line is expected at a wavelength of 391.4 nm. It is a transition within the molecular ion N_2^+ with a lifetime[1] of 60 ns and, therefore, the beam's space charge will interact with the excited gas molecules and distort the observed distribution. The result of a simulation of the distortion caused by one nominal LHC bunch is shown in Fig. 2. The distortion increases the rms width of the observed distribution from 350 µm to 490 µm. In the case of a bunch train the distortion reaches 570 µm. For more simulations of space-charge distortions see [11].

Argon gas has two fluorescence peaks close to each other at 454.5 nm and 476.5 nm. Using a wider optical filter to capture both peaks allows for a total light yield that is between nitrogen and neon at the expense of a higher background. The transitions are ionic and therefore subject to space-charge induced distortion but thanks to the short lifetime[1] of 6 ns and larger atomic mass compared to nitrogen the distortion is minimal.

For more information on the comparison of different working gasses using a Gaussian electron beam see [3].

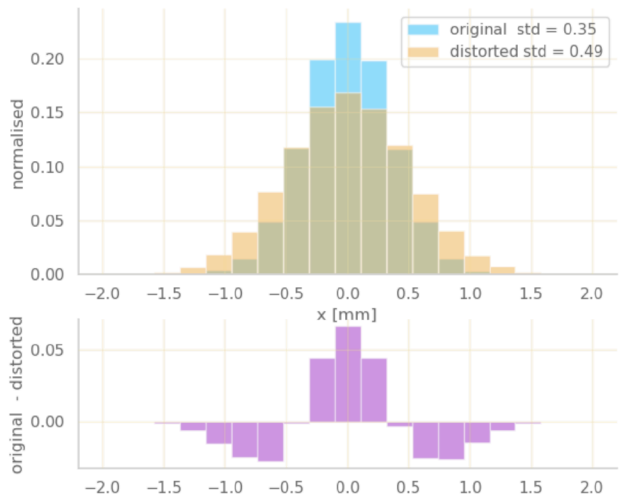

Figure 2: Space charge effect on observed horizontal distribution of one nominal LHC bunch for a thin nitrogen curtain.

BGC Description

The supersonic gas curtain is created by letting the gas to expand into vacuum through a small nozzle and (partly) propagate through a set of skimmers that ensure a low transverse temperature within the jet thus obtained. The third skimmer is rectangular giving the jet its final curtain shape. The gas is in a molecular flow regime, allowing the jet to retain its rectangular cross-section throughout the path across the beam pipe. After crossing the particle beams the jet is pumped out in a dump chamber, which is separated from the interaction chamber by a fourth skimmer to limit back-scattering of gas molecules and therefore minimise the pressure in the interaction chamber.

Part of the photons created by fluorescence get focused by a 40 mm dia., 160 mm focal length apochromatic lens triplet onto a band-pass filter and are finally detected by an intensified camera. The optical band-pass filter limits photons to the wavelengths of interest, e.g. 585 ± 10 nm in the case of Ne. The intensified camera employs double-stage Micro Channel Plate (MCP) amplification allowing for single photon detection.

The observed fluorescent light yield N_γ is given by:

$$N_\gamma = Z \cdot \sigma \cdot \frac{I \cdot \Delta t}{e} \cdot n \cdot d \frac{\Omega}{4\pi} \cdot T \cdot T_f \cdot \eta_{\mathrm{pc}} \cdot \eta_{\mathrm{MCP}}, \quad (4)$$

where σ is the fluorescence cross-section, I the beam current, Δt the integration time, Z the charge state of the passing particle, e the elementary charge, n the curtain's gas density, d the curtain's effective thickness, Ω the acceptance solid angle of the optical system, T the transmittance of the optical system including flange window, T_f the transmittance of the optical filter, η_{pc} the quantum efficiency of a photocathode, and η_{MCP} the efficiency of a the MCP.

Profile Broadening Due to Curtain Thickness

The thickness of the gas jet curtain causes a broadening of the observed vertical beam profile, since fluorescence is produced in the whole volume of the curtain crossed by the beam. Assuming rotational symmetry for the beam and curtain homogeneity in the horizontal plane, the effect can be modelled in 2D. In the case of the BGC the observed profile $I(y)$ is then [10]:

$$I(y) = \int_{-d/2}^{d/2} \rho(\xi)\phi(y - \frac{2}{\sqrt{2}}\xi)d\xi, \quad (5)$$

where ρ is the gas curtain density, ϕ the beam flux, d the gas curtain thickness, ξ the integration coordinate across the curtain's thickness, and y the coordinate along the camera's detector, which in 2D is represented by a line.

Figure 3 shows simulations of profile broadening for a Gaussian beam of rms width σ_{beam} due to a uniform gas curtain. For a curtain thickness $d = \sigma_{\mathrm{beam}}$ and $d = 2 \cdot \sigma_{\mathrm{beam}}$, the observed σ is $\approx 1.08 \cdot \sigma_{\mathrm{beam}}$ and $1.37 \cdot \sigma_{\mathrm{beam}}$, respectively. In the case of the BGC at LHC, the skimmer thickness is $d = 2.7\sigma_{\mathrm{beam}}$, causing a broadening of the vertical distribution of 61 %, as expected. This is acceptable due to the fact that the BGC was conceived as an overlap monitor for the HEL at LHC, where the centroid rather than the profile of the transverse distribution is to be determined. In order to accurately reconstruct the vertical profile, the thickness

[1] Average time between excitation and emission of relevant photon.

ISBN: 978-3-95450-236-3 ISSN: 2673-5350 doi:10.18429/JACoW-IBIC2023-WE3I01

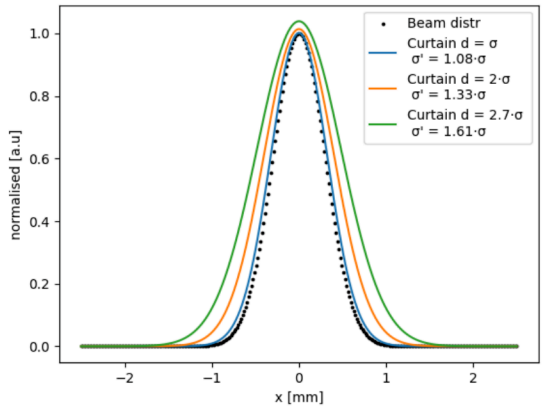

Figure 3: 2D estimations of a vertical beam profile broadening due to finite gas curtain thickness. The beam distribution was chosen to be Gaussian with $\sigma = 0.3$ mm. The gas distribution was homogeneous within thickness d.

of the skimmer should be minimised and the broadening accurately modelled for a realistic gas curtain profile.

For more detailed information see [10] and for simulations of hollow beam profile broadening see [11].

GAS CURTAIN MEASUREMENTS

During the initial testing of the BGC in the lab at Cockcroft Institute, the interaction chamber was replaced with a special chamber containing a movable pressure gauge as shown in Fig. 4. An ion gauge is enclosed within a small chamber with a 1 mm pinhole in the direction of the gas jet. This experimental setup allows for gas density measurements within the portion of the gas jet that interacts with the beam. For more details see [12, 13].

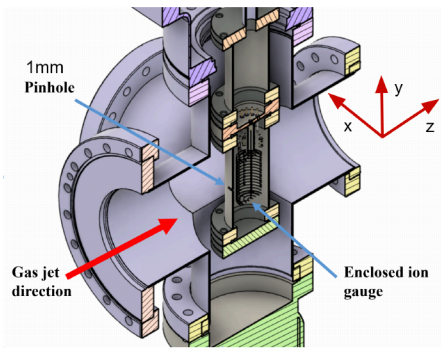

Figure 4: Movable pressure gauge 3D model showing the enclosed ion gauge which is then attached to a stepper motor for each direction. The gas density is sampled through a 1 mm pinhole [12].

The measured transverse density profiles of N_2 and Ne gas jets as obtained with a 0.7 mm thick 3rd skimmer are shown in Fig. 5 plots a) and b), respectively. Both distributions exhibit a good density uniformity. The effective curtain lengths are 12.5 ± 0.5 nm for N_2 and 12.7 ± 0.6 nm for Ne. There are no obvious differences between the shapes of the two profiles, both their lengths and thicknesses agree within measurement errors. As mentioned earlier, the maximum density is larger in the case of Ne, which is due to the difference in the number of degrees of freedom between Ne atoms and N_2 molecules.

Figure 5 plot c) shows the density profile of a nitrogen curtain obtained with a 0.7 mm thick 3rd skimmer. Using the smaller skimmer reduces the maximum density by ≈25 % as well as its effective length down to 10.7 ± 0.7 nm. This, combined with a reduced profile thickness, FWHM of 11.7 ± 0.02 nm, will reduce the fluorescence light yield. However, as experimentally observed at the EBTS, the smaller skimmer leads to a lower background pressure of $8.63 \cdot 10^{-8}$ mbar with respect to the one of $2.04 \cdot 10^{-7}$ mbar due to the larger one. This compensates the lower signal. In addition, a lower thickness also reduces profile broadening, as pointed out in the previous section.

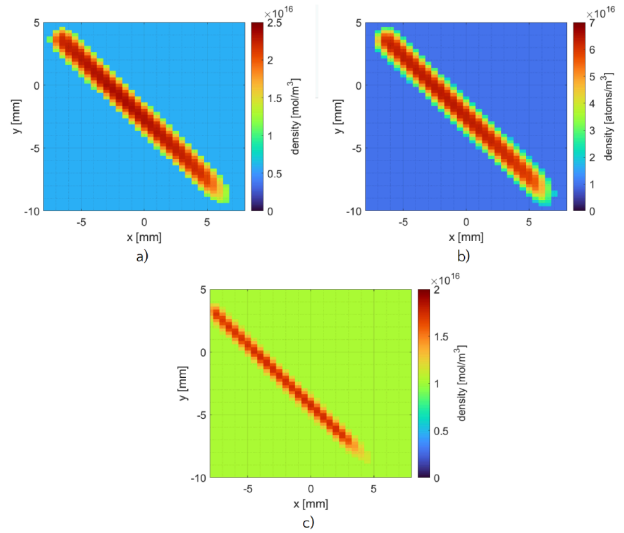

Figure 5: Gas curtain density measurements using a movable pressure gauge. Each pixel corresponds to a position of the movable pressure gauge. a) N_2 curtain using 0.7×9 mm 3rd skimmer. b) Ne curtain using 0.7×9 mm 3rd skimmer. c) N_2 curtain using 0.3×9 mm 3rd skimmer.

EXPERIMENTS WITH HOLLOW ELECTRON BEAMS

The EBTS currently serves as a test stand for the HEL. The BGC was installed at the EBTS to validate its ability to measure a 7 keV hollow electron beam with up to 5 A peak current. The electron beam is magnetized by immersion in a magnetic field and then guided further in a solenoid field. The outer and inner radius of the electron beam can be varied by changing the magnetic field strengths.

Figure 6 shows BGC measurements of the hollow electron beam's transverse profile with different gases. The electron beam was pulsed with a peak intensity of 1.5 A, a 25 µs pulse duration and a 10 Hz repetition rate. Nitrogen, neon and argon were used as working gases and the effective integration time was equivalent to 2 s of a DC beam. The

ISBN: 978-3-95450-236-3 ISSN: 2673-5350 doi:10.18429/JACoW-IBIC2023-WE3I01

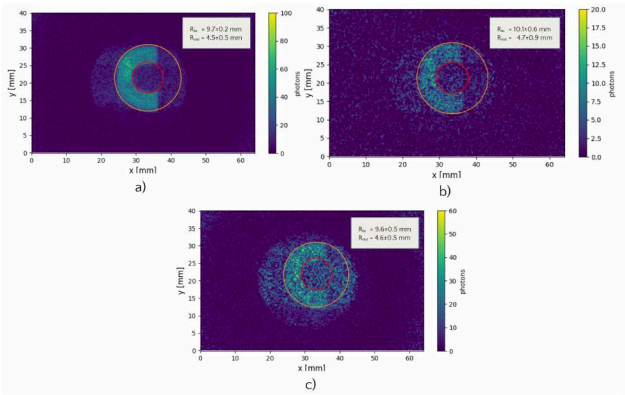

Figure 6: Beam gas curtain measurements of hollow electron beam transverse profile. Nitrogen a), neon b), and argon c) were used as a working gas.

e-beam radii determined with each gas agree within the measurement errors. As expected, the light yield of the nitrogen curtain was the highest, leading to the best image quality. Neon curtains show the lowest light yield, while the higher one of argon curtains is accompanied by a stronger background. This is due to the wider bandwidth of the optical filter used for Ar to allow for integration over several spectral peaks.

The size of the beam was larger than that of the curtain, therefore the distribution could be measured only partially. This allowed for the measurement of the effective curtain size. The 3rd skimmer used for this measurements was 0.3×9 mm and the measured curtain effective length, 12.1 ± 0.3 nm, was larger than expected from measurements with the movable pressure gauge shown in Fig. 5 c). However, it was observed that the exact width of the curtain slightly changes from one alignment of the nozzle and skimmers to another which could explain the 1.4 mm difference.

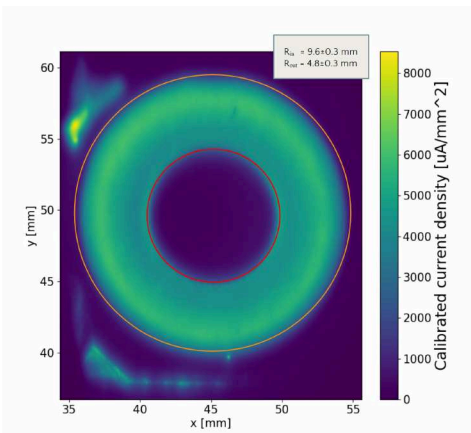

Figure 7: Transverse profile of a 7 keV, 1.1 A peak intensity hollow electron beam as measured with an OTR screen. The profile was averaged over 100 beam pulses of 25 µs duration each.

To benchmark the profiles measured by the BGC, an optical transition radiation (OTR) screen was installed in its place. Glassy carbon was the material of choice to sustain the high charge density. The OTR signal was observed with a single-stage intensified camera. Figure 7 shows a transverse beam profile of a 7 keV, 1.1 A peak intensity pulsed hollow electron beam, featuring 25 µs long pulses. The integration time was equivalent to 2.5 ms of DC electron beam. The observed distribution is rather smooth with a higher current density towards the outer edge of the profile. The measured beam size agrees with the BGC measurements. However, due to a technical fault within one of the power supplies, the magnetic field around the electron gun was 25 % lower than in the case of the EBTS measurements resulting in a smaller transverse profile. This might be explained a slight, but visible, ellipsoid shape of the observed distribution which might be a measurement arte. For more OTR measurements of hollow electron beams taken during another experimental campaign see [14].

EXPERIMENTS WITH LHC PROTON BEAMS

In 2022, BGC collaboration installed and operated an experiment at the LHC where Ne was injected in the beam pipe. Figure 8 a) shows the installation. The preliminary results and details of the installation were presented in Ref. [15]. In 2023, the gas jet was installed at the same position, completing the installation of the BGC at the LHC, as shown in Fig. 8 b).

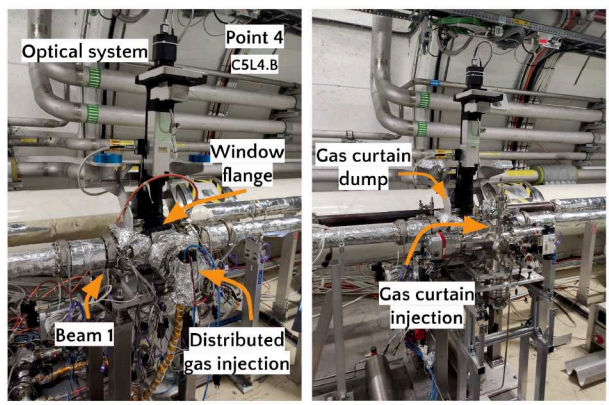

Figure 8: a) Distributed neon fluorescence experiment installation at LHC Point 4. b) Beam Gas curtain installation at LHC Point 4.

Distributed Gas

In the distributed gas experiment, a local pressure bump of several meters in length was created in one of the LHC's beam pipes by injecting neon until a peak pressure of $2.2 \cdot 10^{-8}$ mbar (Ne corrected) was reached. The fluorescence photons were captured by an optical system consisting of an apochromatic lens triplet, a band-pass filter at 585 ± 10 nm and a double-stage MCP intensified camera for single photon detection.

ISBN: 978-3-95450-236-3 ISSN: 2673-5350 doi:10.18429/JACoW-IBIC2023-WE3I01

Figure 9 shows a result from the fluorescence campaign. This is a measurement of a full LHC beam with $1.5 \cdot 10^{14}$ protons and an integration time of 430 s. The expected cross-section was estimated to be $4.7 \cdot 10^{-22}$ cm^2 in accordance with [10].

Table 1: The optical system parameters of the BGC and distributed gas experiment. The quantum efficiency of the photocathode corresponds to the sensitivity around wavelengths of 585 nm. Units for optical acceptance are 4π Sr.

Parameter	Value
Optical acceptance	$1.43 \cdot 10^{-3}$
QE of Photocathode	0.09
MCP efficiency	0.75
Transmittance of filter	0.80
Trans. of opt. system	0.85

Based on this expected cross-section and datasheet parameters of the optical system efficiencies, as summarised in Table 1, the expected light yield was 2.5x higher than observed. This is rather good agreement with respect to the fact that only data points at very low energies were available for the extrapolation of the expected cross-section. Several sanity checks were performed to ensure the validity of the signal. The signal rose with the integration time roughly linearly. Turning off the gas injection caused the signal peak to vanish as expected. Lastly, varying the position of the optical system distance along its optical axis did show that the beam is in focus.

The gas injection was validated also against increased beam losses or any other effect on the beam. No visible additional losses above the noise were observed by the LHC operators, deeming the gas injection transparent for the beam.

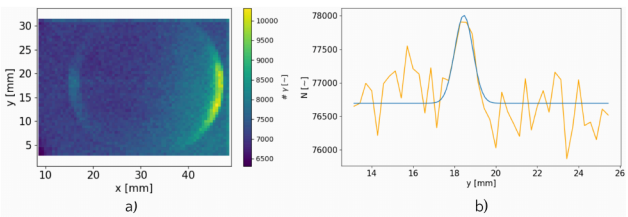

Figure 9: Ne fluorescence measurements at LHC with distributed gas. a) Observed 2D distribution showing the LHC beam horizontally across the field of view and a bright ring of synchrotron radiation. b) The horizontal profile of the LHC beam [15].

BGC at LHC

At the beginning of 2023, the full BGC was installed at the LHC, replacing the distributed gas injection with a neon gas curtain injection and dump chamber.

Testing the gas curtain at LHC increased the background pressure up to roughly $4 \cdot 10^{-8}$ mbar. This is an acceptable local background pressure level for the LHC. The monitor operation with gas curtain injection was validated and deemed acceptable for a safe operation of the LHC. The validation was done during beam injection, energy ramp from 450 GeV to 6.8 TeV and finally collisions, i.e. for the whole standard LHC fill.

The measured neon gas curtain density is equivalent to a pressure of $3.31 \cdot 10^{-6}$ mbar at room temperature. This constitutes an increase of the local gas density by a factor of 150.5. The smaller 0.3×9 mm 3rd skimmer was installed to limit the gas load onto the LHC vacuum and improve the background pressure. This choice, in comparison to the larger 0.7×9 mm 3rd skimmer, reduces the gas jet thickness by a factor of ≈2, and the curtain density by ≈25 %, but also it's broadening effect. The gas curtain installation allowed for minimally invasive 2D distribution measurements with a significant integration time decrease. The first results are currently being analysed.

CONCLUSIONS

This paper presents the BGC, a two-dimensional profile monitor utilizing the fluorescence of a supersonic, curtain shaped gas jet. The curtain density profile was measured for neon and nitrogen as well as for two sizes of the 3rd skimmer. The densities show good transverse uniformity. On the EBTS, the transverse profile of the hollow electron beam was measured using nitrogen, neon, and argon gas curtains. The measured beam radii for each gas are in agreement. Furthermore, a hollow electron profile measurement using the OTR method was shown. Fluorescence induced by 6.8 TeV proton beam at LHC was measured during distributed gas experiments. The results show a faint signal of the beam. The BGC was installed at the LHC for two-dimensional profile observations of the LHC beam. The first measurements show a significantly increased signal-to-noise ratio compared to previous fluorescence experiments at the LHC. The monitor was validated with the LHC beam and deemed safe for LHC operation. The BGC is now in operation at the LHC for characterisation with ultra-high energy proton and lead beams.

ACKNOWLEDGMENTS

This work was supported by STFC under grant agreement ST/P006752/1 and is a part of the HL-LHC project.

REFERENCES

[1] A. Giorgio *et al.*, "High luminosity large hadron collider HL-LHC", *arXiv*, 2017. doi:10.48550/arXiv.1705.08830

[2] S. Udrea *et al.*, "Development of a Fluorescence Based Gas Sheet Profile Monitor for Use With Electron Lenses: Optical System Design and Preparatory Experiments", in *Proc. IBIC'17*, Grand Rapids, MI, USA, Aug. 2017, pp. 359–363. doi:10.18429/JACoW-IBIC2017-WEPCC08

[3] A. Salehilashkajani *et al.*, "A gas curtain beam profile monitor using beam induced fluorescence for high intensity charged particle beams", *Appl. Phys. Lett.*, vol. 120, no. 17, 2022. doi:10.1063/5.0085491

ISBN: 978-3-95450-236-3 ISSN: 2673-5350 doi:10.18429/JACoW-IBIC2023-WE3I01

[4] A. Salehilashkajani *et al.*, "Commissioning of the Prototype for a New Gas Curtain Beam Profile Monitor Using Beam Induced Fluorescence for HL-LHC", in *Proc. IPAC'19*, Melbourne, Australia, May 2019, pp. 2709–2712. doi:10.18429/JACoW-IPAC2019-WEPGW093

[5] V. Tzoganis and C.P. Welsch, "A non-invasive beam profile monitor for charged particle beams", *Appl. Phys. Lett.*, vol. 104, no. 20, p. 204104, 2014. doi:10.1063/1.4879285

[6] H.D. Zhang *et al.*, "A Supersonic Gas-Jet Based Beam Induced Fluorescence Prototype Monitor for Transverse Profile Determination", in *Proc. IPAC'17*, Copenhagen, Denmark, May 2017, pp. 458–461. doi:10.18429/JACoW-IPAC2017-MOPAB139

[7] H.D. Zhang *et al.*, "A Supersonic Gas Jet-Based Beam Profile Monitor Using Fluorescence for HL-LHC", in *Proc. IPAC'18*, Vancouver, Canada, Apr.-May 2018, pp. 1891–1894. doi:10.18429/JACoW-IPAC2018-WEPAF034

[8] A. Rossi *et al.*, "DC and Pulsed Electron Beam Test Facility at CERN", in *Proc. IPAC'23*, Venice, Italy, May 2023, pp. 1953–1956. doi:10.18429/JACOW-IPAC2023-TUPL104

[9] R. Hampf, J. Wieser, and A. Ulrich, "Light emission processes in the context of optical beam profile monitors", in *Eur. Phys. J.*, vol. 77, no. 51, 2023. doi:10.1140/epjd/s10053-023-00624-6

[10] S. Udrea and P. Forck, "Milestone1.1, 1.2, and 1.6 report", GSI, Darmstadt, Germany, 2018, Report No. CERN-EDMS-2333411 and CERN-EDMS-2333413.

[11] O. Sedlacek *et al.*, "Simulations of Space-Charge and Guiding Fields Effects on the Performance of Gas Jet Profile Monitoring", in *Proc. IPAC'21*, Campinas, Brazil, May 2021, pp. 898-901. doi:10.18429/JACoW-IPAC2021-MOPAB283

[12] H.D. Zhang, A. Salehilashkajani, O. Sedlacek, and C.P. Welsch "Characterization of a supersonic gas jet for charged particle beam profile monitor", *arXiv*, 2022. doi:10.48550/arXiv.2205.05386

[13] H.D. Zhang *et al.*, "Imaging a high-power hollow electron beam non-invasively with a gas-jet-based beam profile monitor", in *Proc. IPAC'23*, Venice, Italy, May 2023, pp. 4529-4532. doi:10.18429/JACoW-IPAC2023-THPL066

[14] O. Sedlacek, M. Sameed, *et al.*, "Optical Transition Radiation Measurements of a High Intensity Low Energy Hollow Electron Beam on Electron Beam Test Facility", in *Proc. IPAC'23*, Venice, Italy, May 2023, pp. 3905-3908. doi:10.18429/JACoW-IPAC2023-THPA002

[15] O. Sedlacek *et al.*, "HL-LHC Beam Gas Fluorescence Studies for Transverse Profile Measurement", in *Proc. IBIC'22*, Kraków, Poland, September 2022, pp. 261–264. doi:10.18429/JACoW-IBIC2022-TUP17